Background Stress State Before the 2008 Wenchuan Earthquake and the Dynamics of the Longmen Shan Thrust Belt

KAIYING WANG,[1] Yu. L. REBETSKY,[2] XIANGDONG FENG,[3] and SHENGLI MA[1]

Abstract—A stress reconstruction was performed based on focal mechanisms around the Longmen Shan region prior to the 2008 M_s 8.0 Wenchuan earthquake using a newly developed algorithm (known as MCA). The method determines the stress tensor, including principal axes orientations, and quantitative stress values, such as the effective confining pressure and maximum shear stress. The results of the MCA application using data recorded by the regional network from 1989 to April 2008 show the background stress state around the Longmen Shan belt before the Wenchuan earthquake. The characteristics of the stress orientation reveal that the Longmen Shan region is primarily under the eastward extrusion of the eastern Tibetan plateau. Non-uniform quantitative stress distributions show low stress levels in the upper crust of the middle Longmen Shan segment, which is consistent with the observed high-angle reverse faulting associated with the 2008 Wenchuan earthquake. In contrast, other study areas, such as the Bayankela block and the NW strip extending to the Sichuan basin, show high stress intensity. This feature coincides with heterogeneity in the wave speed image of the upper crust in this region, which shows high S-wave speed in the high stress areas and comparatively low S-wave speed in low stress areas. Deformation features across the Longmen Shan belt with the slow rates of convergence determined by GPS and the distribution of surface deformation rates also are in keeping with our stress results. We propose a dynamic model in which sloping uplift under the Longmen Shan, which partly counteracts the pushing force from the eastern plateau, causes the low-quantitative stresses in the upper crust beneath the Longmen Shan. The decreasing gravitational potential energy beneath the Longmen Shan leads to earthquake thrust faulting and plays an important role in the geodynamics of the area that results from ductile thickening of the deep crust behind the Sichuan basin, creating a narrow, steep margin.

Key words: Wenchuan earthquake, deformation features, MCA, quantitative stress, background stress state, low stress level, sloping uplift.

1. Introduction

The devastating May 12, 2008 Wenchuan earthquake (M_w 7.9) occurred beneath the eastern margin of the Tibetan plateau, rupturing the central high-angle Longmen Shan thrust fault (Fig. 1). This observation raises an important question: what geodynamics are responsible for this special type of strong earthquake? The answer to the question is closely related to recent tectonic deformation of the eastern Tibetan plateau, which is characterized by eastern expansion as a result of the continent–continent collision of India with Eurasia. For several years, there has been controversy regarding the style of the lateral expansion of the eastern Tibetan Plateau. The argument is that the plateau may deform either by movement of rigid crustal blocks along large strike-slip faults (Tapponnier et al. 1982; Tapponnier et al. 2001), by continuous deformation (Houseman and England 1993; Copley 2008), or by the eastward flow of viscous lower crust (Royden et al. 1997, 2008).

There should be different geodynamics and measured stress states in the Longmen Shan tectonic zone corresponding to these different deformational models. The first two include extrusion along the left-lateral strike-slip faults that slice Tibet's east side or a continuous deformation style in which vertical planes deform by pure shear, and there are no vertical gradients of horizontal velocity. From these two styles, it can be inferred that the Longmen Shan tectonic zone is primarily subject to a horizontal pushing force, that the stress orientation should be consistent from the shallow to deep crust, and that there should be little change in stress intensities when lithostatic pressure is taken off. In contrast, in the lower crustal flow model, deep crustal material moves eastward from middle Tibet around the

[1] State Key Laboratory of Earthquake Dynamics, Institute of Geology, China Earthquake Administration, P.O. Box 9803, Beijing 100029, China. E-mail: wangky@ies.ac.cn

[2] Institute of Physics of the Earth, Russian Academy of Sciences, Moskva 123810, Russia.

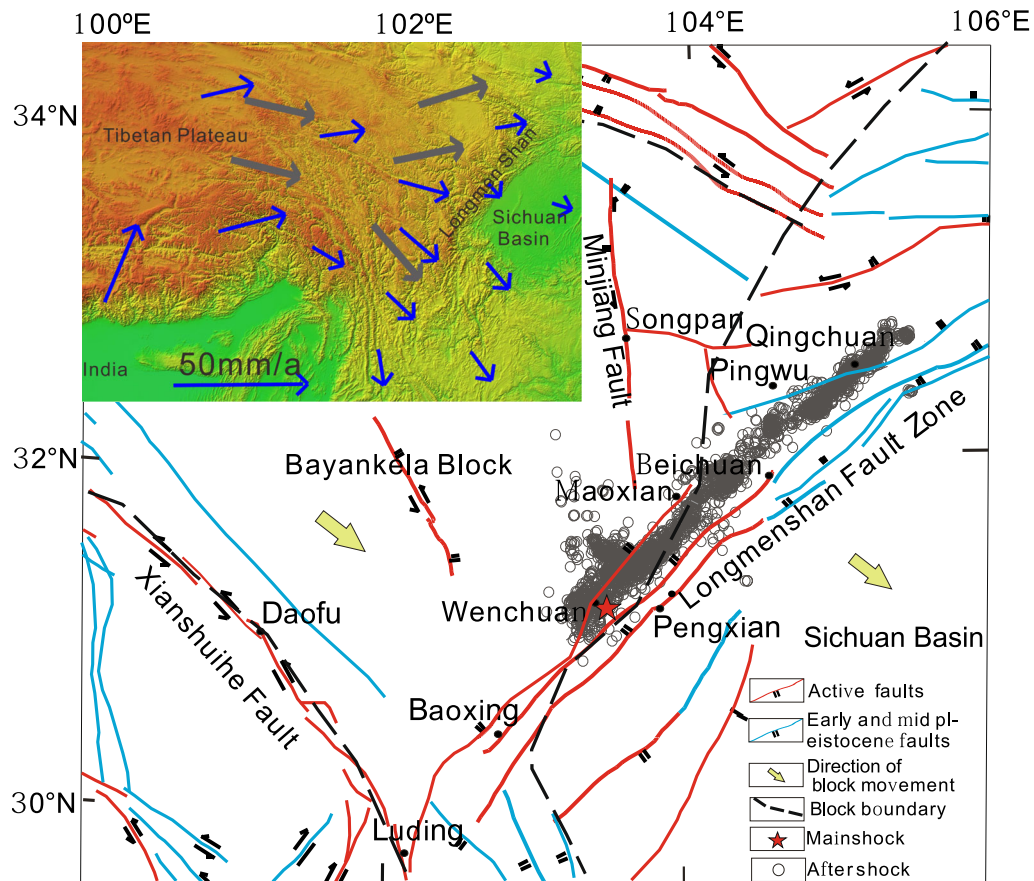[3] Earthquake Administration of Hebei Province, Shijiazhuang 050012, China.

Birkhäuser

Figure 1
Sketch of the active tectonics in the Longmen Shan region including epicenters of the 2008 M_w 7.9 Wenchuan earthquake sequence. In the top left corner blue arrows indicates GPS velocity vectors and gray arrows shows crustal flow

strong crust of the Sichuan basin and accumulates behind the basin. In this model, there is an obvious difference between the stress state in the upper crust and the deep crust under the Longmen Shan, and the uplift of the material piling up plays an important role in the geodynamics of the area.

The Longmen Shan has numerous geological features atypical of active convergent mountain belts (Burchfiel et al. 2008; Kirby et al. 2008), including that young high mountains reach more than 4000 m relief without adjacent foreland subsidence. Analysis of GPS velocity data (Wang et al. 2015; Zhang et al. 2008) shows that the shortening rate across the Longmen Shan is less than 3 mm/year, which is an order of magnitude lower than the crustal strain rate in the adjacent Xianshuihe fault. Rapid uplift and

slow horizontal pressing indicate that the horizontal driving force in the upper Longmen Shan crust is weak. Coseismic deformation associated with the 2008 Wenchuan earthquake occurred mostly within the Longmen Shan fault zone and decreased very rapidly away from the surface rupture zone (Xu et al. 2009; Liu-Zeng et al. 2009). Aftershocks have been confined to a particularly narrow belt along the Longmen Shan fault zone. These characteristics suggest that the horizontal force from the eastern Tibet acting on the Longmen Shan is not the dominant cause of the high-angle reverse faulting and tectonic deformation in the upper crust.

Clark and Royden (2000) proposed that crustal thickening in eastern Tibet occurs largely within a weak (low-viscosity) zone in the mid- to lower crust.

For an assumed 15-km-thick channel, Newtonian fluid model results indicate that crustal flows create the broad, gentle margins of eastern plateau and accumulate behind the Sichuan basin, creating a narrow, steep margin. Zones of weakness in the deep crust that thicken eastwards towards the craton beneath the Sichuan basin have been identified from structural imaging and interpreted as crustal flow channels (Liu et al. 2014). This interpretation can be tested by determining whether that the upper Longmen Shan crust is in a low horizontal stress, implying that the eastward pushing force of the Tibetan plateau in the upper crust acting on the Longmen Shan is small and dose not completely account for the Wenchuan earthquake.

To characterize the geodynamics of the Longmen Shan belt, it is important to know the stress state at seismogenic depths in the upper crust, where we propose a low stress level. In situ stress measurements using a hydro-fracturing technique were obtained in the northeastern Longmen Shan belt after the 2008 earthquake, indicating that the stress values at several depths within the Longmen Shan faults are considerably lower than those at Pingwu, which is located at hanging wall northwest of the Longmen Shan (Chen et al. 2012). However, because of the small number of measurement points and the limited depth of 400 meters, the stress intensity of the Longmen Shan belt at seismogenic depth remains poorly understood.

The abundance of small earthquakes offers many different focal mechanisms, which can be used to obtain principal stress axes orientations in different sub-regions under the assumption of uniform stress. The most commonly used approaches for obtaining principal stress axes orientations are described by Angelier (1979, 1989), Ellsworth and Xu (1980), Gephart and Forsyth (1984), Michael (1987), and Xu et al. (1992). Other methods for estimating deviatoric stress magnitudes using focal mechanisms before and after an earthquake and coseismic stress change have been proposed (Wan et al. 2006; Hardebeck 2012; Yang et al. 2013).

2. Method

As a continuation of the work of Angelier and others, a method of cataclastic analysis called MCA, involving two basic steps, was developed to determine complete stress tensor components based on earthquake focal mechanisms (Rebetsky et al. 2012, 2016). The orientation of the principal stress axes and the Lode–Nadai coefficient or stress ratio, which characterizes the shape of the stress ellipsoid, are evaluated during the first stage of the MCA. The first stage also involves identifying a homogeneous sample set of earthquake focal mechanisms that characterizes the quasi-homogeneous deformation of a specific crustal domain.

The procedures in the first stage are very similar to those in the classical method developed by Angelier (1989, 1990), Carey-Gailhardis and Mercier (1987), and Gushchenko and Kuznetsov (1979). The procedures for generating homogeneous samples of earthquake focal mechanisms are based on inequalities that are similar to the one used in the right dihedral method by Angelier and Mechler (1977). In this study, the homogeneous sample includes events where the quadrants formed by the nodal planes intersect. This is equivalent to requiring that the irreversible plastic deformations of elongation and shortening along a principal axis due to each earthquake (α) are defined according to the axis' index. Elongation accumulates only along the σ_1 axis (minimum compression), and shortening accumulates only along the σ_3 axis (maximum compression). Therefore,

$$d\varepsilon_{11}^{\alpha} \geq 0, \quad d\varepsilon_{33}^{\alpha} \geq 0. \tag{1}$$

σ_1 and σ_3 correspond to the algebraically largest and smallest of the principal stresses, respectively.

Instead of the inequalities in Eq. (1), the MCA has

$$d\varepsilon_{11}^{\alpha} \geq d\varepsilon_{22}^{\alpha} \geq d\varepsilon_{33}^{\alpha} \tag{2}$$

$$d\varepsilon_{11}^{\alpha} + d\varepsilon_{22}^{\alpha} + d\varepsilon_{33}^{\alpha} = 0, \tag{3}$$

where $d\varepsilon_{ii}^{\alpha}$ are components of increment of plastic deformations of elongation and shortening in directions of principal stress axis σ_i ($i = 1, 2, 3$) after earthquake number α from a homogeneous sample.

Condition (2) is a consequence of the ordering principle of the development of irreversible deformations used in the theory of plasticity. This principle follows from the postulate of maximum plastic dissipation (Mises 1928). Correct stresses are those that

maximize the elastic energy dissipation for a known irreversible deformation tensor.

In the MCA, inequality (2) is assumed as the criterion for compiling homogeneous sets of earthquake mechanisms that are used to define the parameters of the stress tensor for quasi-homogeneous domains. After the right dihedral method (Angelier and Mechler 1977), using expression (2) and data on earthquake mechanisms, it is possible to locate the principal stress axes of the desired stress tensor on the unit hemisphere areas.

After the first stage of the MCA, out of six components of stress tensor, the confining pressure p and the module of maximal shear stress τ are left undefined. The approach to determining the effective isotropic pressure $p*$ (tectonic pressure without fluid pressure) and maximum shear stress τ is based on experiments on the brittle fracture of rock samples (Byerlee 1968, 1978), according to which a brittle fracture band is allocated on the Mohr diagram (Rebetsky et al. 2012). All points on Mohr's diagram characterizing the critical state on newly developed and re-activated cracks fall into the area between upper yield envelope (inner brittle strength) and the bottom line of resistance to static friction with minimal—zero cohesion (Fig. 2).

At second stage of the MCA, after calculating the reduced stresses from a homogeneous sample, and applying the corresponding points to the Mohr diagram, we can estimate the effective pressure p^{eff} and maximum shear stress τ normalized to the unknown cohesive strength (T_f) of the rock massif (Rebetsky et al. 2012, 2016).

$$\frac{p^{\text{eff}}}{\tau_f} = \frac{\left(\tilde{\sigma}_{nt}^K - k_s \tilde{\sigma}_{nn}^K - k_s \mu_\sigma/3\right)}{k_s[\sec(2\beta_s) - (\tilde{\tau}_{ns}^K - k_s \tilde{\sigma}_{nn}^K)]};$$
$$\frac{\tau}{\tau_f} = \frac{1}{\sec(2\varphi_s) - (\tilde{\sigma}_{ns}^K - k_s \tilde{\sigma}_{nn}^K)}. \qquad (4)$$

$\tilde{\sigma}_{nn}$ and $\tilde{\tau}_n$ are the corresponding reduced shear stress and effective normal stress acting on the crack plane from homogeneous sample of slip fault sets:

$$\tilde{\sigma}_{nn} = (\sigma_{nn} + p^{\text{eff}})/\tau = (1 - \mu_\sigma)(n_1^l)^2 - (1 + \mu_\sigma)(n_3^l)^2 + 2\mu_\sigma/3;$$
$$\tilde{\tau}_n = \tilde{\sigma}_{nt} = \sigma_{nt}/\tau = (1 - \mu_\sigma)n_1^l t_1^l - (1 + \mu_\sigma)n_3^l t_3^l; \qquad (5)$$

where $\tau = (\sigma_1 - \sigma_3)/2$, $p = -(\sigma_1 + \sigma_2 + \sigma_3)/3$, $p^{\text{eff}} = p - p_{\text{fl}}$, $\beta_s = \frac{1}{2}\arctan\frac{1}{k_s}$, $\varphi_s = \arctan k_s$, k_s
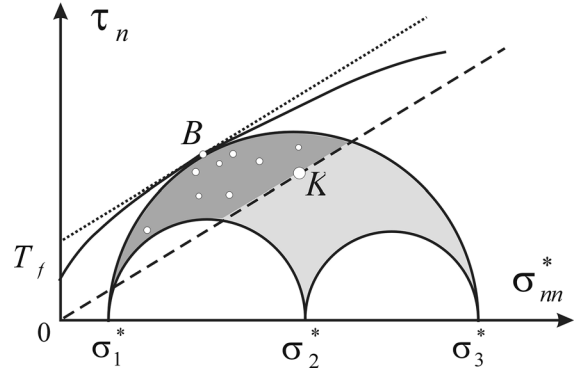

Figure 2
Zone of brittle destruction on Mohr diagram. The simplified form of a zone of the brittle destruction, are used in MCA algorithm. Solid line is Mohr failure envelope for real geo-material. Upper dotted direct line corresponds to the approximation of the Mohr failure envelope curve. Lower long-dashed line corresponds to the minimum of static friction stresses. Area of light gray color inside the big and above small circles of Mohr, defines stress states on the different orientation planes. Area of dark gray color means failure zone for restriction. Points within dark gray area are normal and shear stresses on the planes of slip faults from a homogeneous sample. The point K lies on the line of the minimum resistance of friction ($i = 1, 2, 3$) and is effective principal and normal stresses accordingly

represents the static frictional coefficient of the faults, μ_σ is the Lode–Nadai coefficient characterizing shape of the stress tensor, n_i and t_i ($i = 1, 2, 3$) are the direction cosines of the displacement vector and the shear stress on the fault plane in a coordinate system referenced to the principal axis of the stress tensor. An approach suggested in Angelier's paper (1989) should be considered to be closest to the MCA algorithm.

3. Data and Application of the MCA

The ratios of S to P amplitudes, as recorded on vertical component seismographs near an earthquake provide a means of determining the focal mechanism at short epicentral distances (Kisslinger 1980; Kisslinger et al. 1981). Systematic variations in S/P amplitude ratios are expected because P-wave amplitudes are large near the P and T axes of the focal mechanism and smaller near the nodal planes, whereas the S-wave amplitudes are largest near the nodal planes. Hardebeck and Shearer (2003) tested that the observed S/P ratios are generally consistent
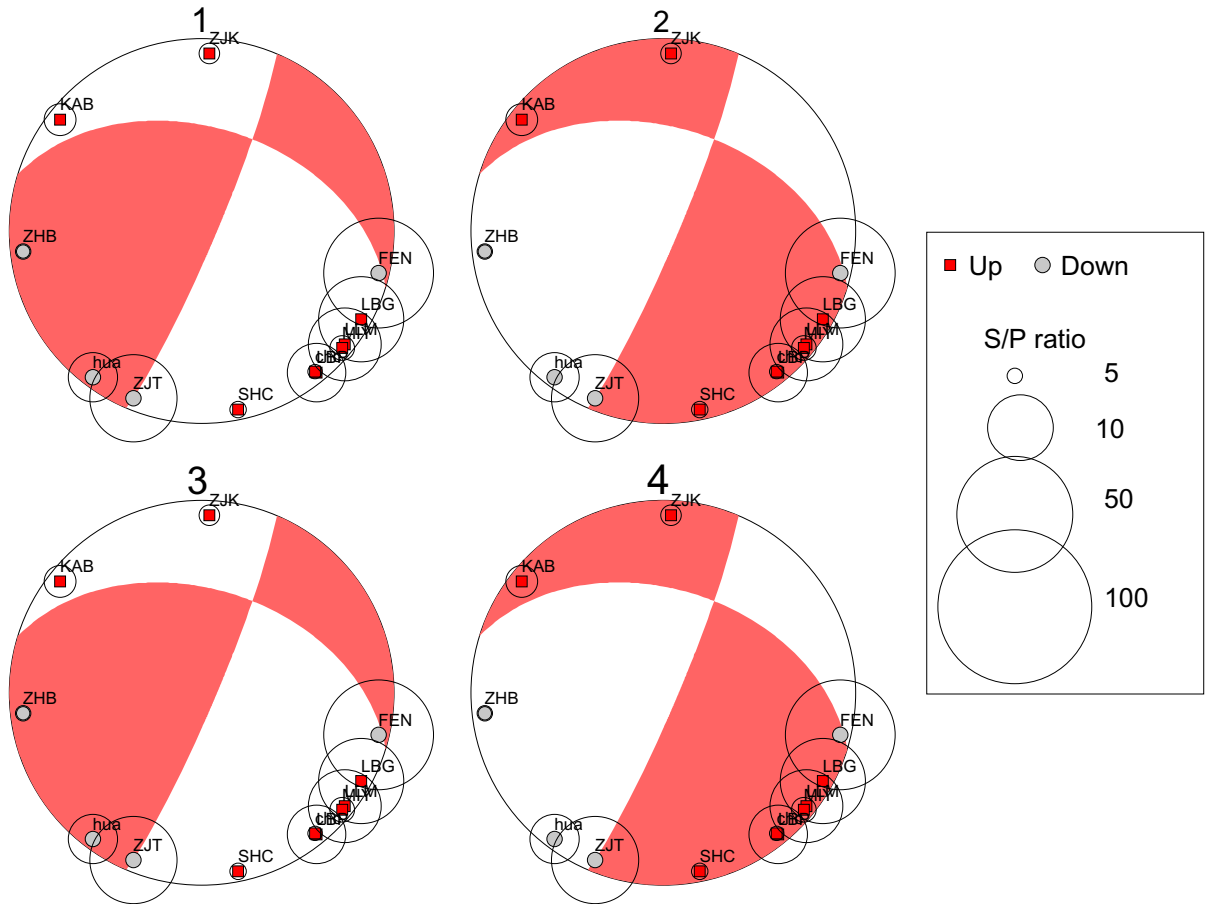
Figure 3

Example showing how to use SV/P amplitudes ratios in addition to P-wave polarities to determine an earthquake focal mechanism

with the expected mechanisms. Others (Snoke et al. 1984; Rau et al. 1996; Shen et al. 1997) developed programs to determine focal mechanism solutions by incorporating P-wave polarities and SV/P amplitude ratios. The use of the amplitude ratio along with polarity can constrain the mechanism solutions more effectively than the use of polarity alone.

Liang and Li (1984) used the SV/P amplitude ratios in addition to P-wave polarities to determine the focal mechanism of small earthquakes. The method calculates theoretical maximum SV/P amplitudes ratios from synthetic seismograms for a point source of dislocation in a planar-layered medium and obtains the best focal parameters by fitting the observed amplitude ratios with the theoretical ones. If the total number of consistent amplitude ratios is within a preset error allowance, then the

solution is accepted. Lin et al. (1991) conducted artificial data tests to prove the reliability of the method, even if the stations are not well distributed. Figure 3 is an example showing how to obtain the desired focal mechanism using the method. The serial numbers 1–4 are the best possible solutions that satisfy a predetermined data consistency criterion. The nodal planes are shown in the beach balls, and the observations are plotted as circles. When P-wave polarities are included, then solution No. 2 or No. 4 is declared to be valid in the example.

Using the method based on SV/P amplitudes combined with P-wave first-motion polarities, focal mechanism solutions were determined for 675 events recorded by at least 6 stations (Fig. 4). These events were from 1989, when the temporal distribution of seismic events was monthly in Sichuan province, to
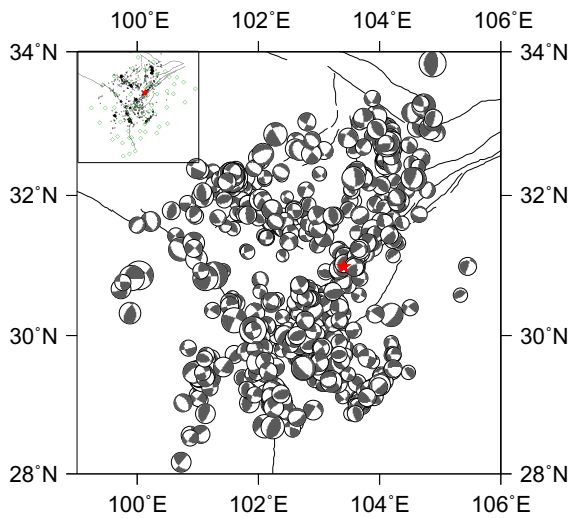
Figure 4
Focal mechanism solutions of small earthquakes recorded between 1994 and April 2008 in the Longmen Shan region. The green diamonds represent locations of station

April 2008, prior to the Wenchuan earthquake. The magnitudes for these focal mechanisms were on the scale of $M_s = 3–5$ and focal depths were distributed from 1 to 25 km. Regional digital seismic stations within Sichuan province are distributed as shown in Fig. 4. The data obtained on the stressed state correspond to the long-period component, that is, they are the average stresses for the whole period of time for the catalog of mechanisms of earthquake foci. Time variations in stresses in this work have not been investigated.

Based on the mechanism solutions, background stress tensors around the Longmenshan belt were reconstructed prior to the Wenchuan earthquake using the MCA. According to the spatial distribution of focal mechanisms and the depths of approximately 1–25 km, the grid size was chosen to be 0.2° × 0.2° located at a 13 km depth, above the 2008 Wenchuan focal depth ($\sim$ 18 km) (Chen et al. 2009). The static frictional coefficient is determined to be 0.6, and rock cohesion to be 0.1 Kbar. Each homogeneous sub-region includes at least six earthquakes, and the maximum radius around a node does not exceed 35 km, which represents the elastic unloading range calculated according to earthquake magnitude (Rebetsky et al. 2012). The maximum radius should not be set too large, even if more stress points will be

obtained, otherwise some earthquakes may influence too large an area. The maximum radius should be chosen according to spatial density of focal mechanism data after several initial calculations.

The results (Fig. 5) include orientations of principal stress axes, stress regimes types, and normalized values of maximum shear stress τ relative to rock cohesion, which can represent the stress level of a unit body on a Mohr diagram. From the orientation of the principal stress axes, it is possible to regionalize the crust based on its geodynamic or stress state regimes. These regimes are defined by the shared orientation of principal stress axes and zenith direction. The types of geodynamic regimes represent the spherical octant including the horizontal extension regime, the horizontal extension with horizontal shear, the horizontal shear regime, the horizontal compression with horizontal shear, the horizontal compression regime, and the vertical shear stress state.

Directions of maximum compressive stresses in the study area are in general agreement with previous estimates (Zoback 1992; Xu et al. 1992; Heidbach et al. 2010). Distribution of the stress regimes, as well as stress axes, indicate that the upper crust of the Longmen Shan region is primarily subject to eastward horizontal compressive forces from the pushing of the upper crust away from the central Tibetan plateau and toward the eastern plateau region.

Normalized maximum shear stresses show that stress levels are very heterogeneous and, in certain areas, are comparatively large. The NW-oriented strip, from the southern Xianshuihe fault to the intersection of the Xianshuihe fault and the Longmen Shan fault, extending southeastwards to the Sichuan basin, corresponds to the highest stress level. In the Bayankela block of eastern Tibet, the stress distribution shows that most of the stresses are very high in magnitude. In contrast to these areas, the Longmen Shan area is characterized by a low stress level, with two localized patches of high stress at both ends.

The high stress distribution in the area intersecting the Xianshuihe fault and the Longmen Shan, and extending southeastward to the Sichuan basin, corresponds to a zone of comparatively high S-wave velocity ($\sim$ 3.9 km/s) at the depth of 10 km in the upper crust (Liu et al. 2014). In addition, stresses
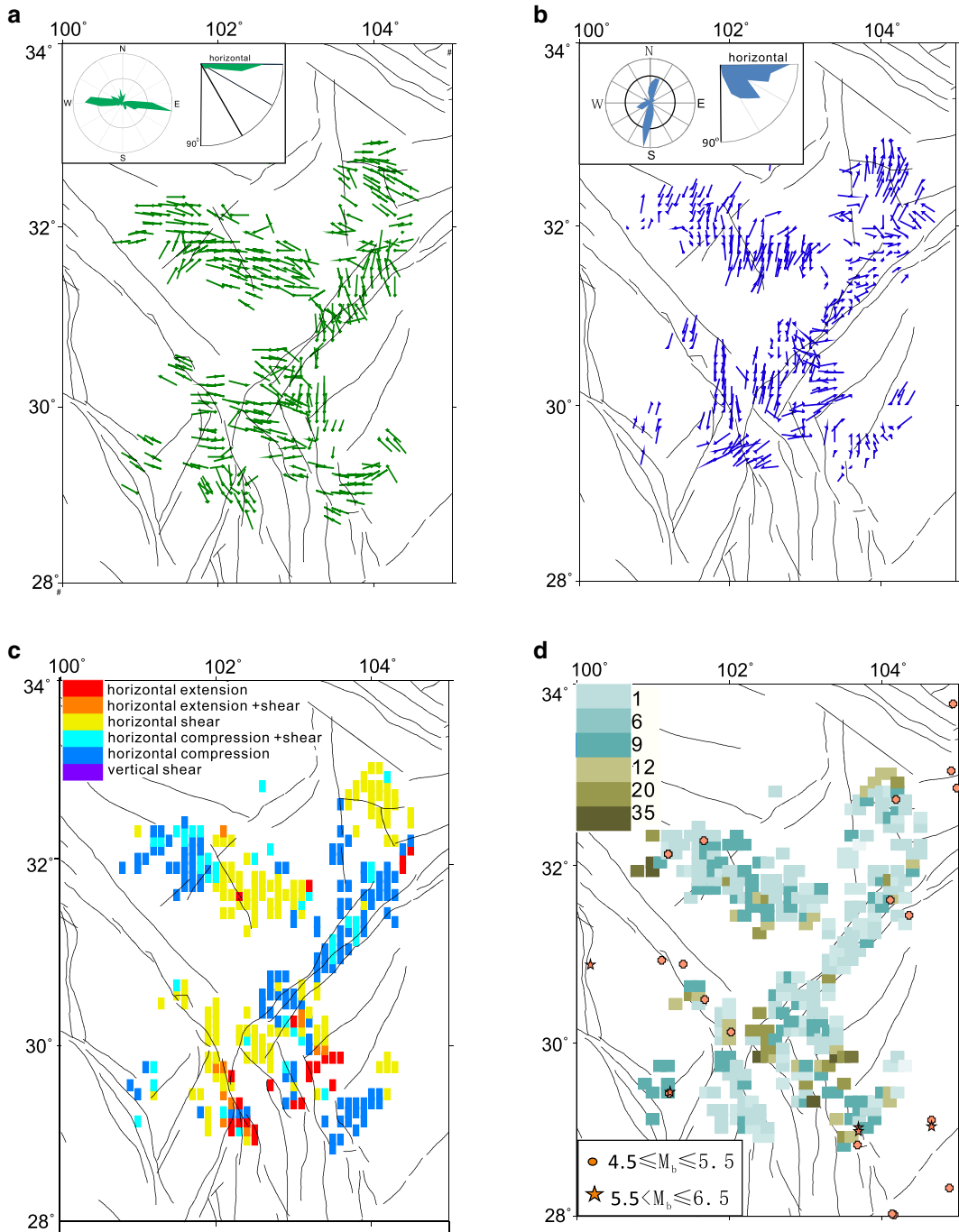
Figure 5
Stress field distribution in the Longmen Shan region: **a** projections of maximum compressive axes in the horizontal plane; **b** projections of maximum extensional axes in the horizontal plane; **c** types of stress regimes: green represents horizontal shear, blue represents horizontal compression, red represents horizontal extension; **d** normalized values of maximum shear stresses

within eastern Tibet are higher than those within the Longmen Shan, similar to the wave speed heterogeneity of 3.7 vs. 3.5 km/s. The two patches of high stress in Longmen Shan also correspond to high wave speeds of approximately 3.7–3.9 km/s.

Similarly, distribution of the geodetic strain rate obtained at the decadal scale in the Sichuan and Yunnan areas shows higher strain rates in the eastern Plateau than in the Longmen Shan (Copley 2008; Wang et al. 2015), and the heterogeneity of the strain rate distribution in west Sichuan is generally consistent with the stress distribution.

The combination of variance of quantitative stress, with wave speed being in the upper crust, and the surface strain rate favors the stress inversion results. From preliminarily comparative analysis, it can be inferred that the change in rock density due to the stress and strain has an important influence on the wave speed variation in the upper crust.

4. Discussion and Conclusions

Orientations of stress axes and geodynamic regimes representative of the stress state at a depth of approximately 13 km beneath the Longmen Shan, as presented above, show that the upper Longmen Shan crust is primarily stressed by the pushing force from the eastern Tibetan plateau. Obviously, low stress levels along the Longmen Shan compared with other areas reveal that material accumulation under the Longmen Shan plays an important role in the geodynamics of the area, which results from ductile thickening of the deep crust behind the Sichuan basin, creating a narrow, steep margin.
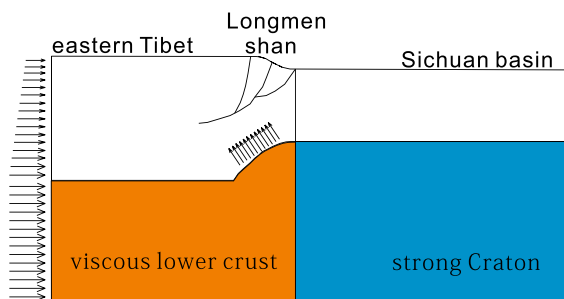
The stress state in the upper crust beneath the Longmen Shan is accommodated by a combination of plateau expansion and sloping uplift of the deeper crust beneath the Longmen Shan. The orientation of the uplift is declining towards northwest as illustrated in the conceptual cartoon (Fig. 6), which is caused by accumulation of material, similar to the decoupled pure-shear crustal thickening model proposed by Feng et al. (2016), where east-dipping ductile shear zones in the depth range ∼ 20 km were revealed by deep-sounding seismic reflection profiling. The uplift in part counteracts the pushing force from the eastern plateau, causing the low-quantitative stresses in the upper crust beneath the Longmen Shan, and reducing the gravitational potential energy beneath the Longmen Shan, leading to earthquake thrust faulting. Geological features such as high mountains reaching more than 4000 m relief, without adjacent foreland subsidence, and with only slow active convergence can also be interpreted from the geodynamics.

Regarding quantitative normalized stresses in the different nodes or areas concerned, it can be seen from Eq. (4) that the effective stress and the maximum shear stress are normalized to rock cohesion τ_f, which may differ for different rock physics and for different scales of stress field. As a result, normalized stresses depend on the tectonic development of a region and its current state, so the acquired stress intensities for the region are only semi-quantitative, and the low stress level in upper Longmen Shan crust may be reduced to a certain extent due to cataclastic fault material or other reasons.

Figure 6
Conceptual cartoon to illustrate geodynamics beneath the Longmen Shan. Scales for the diagram is arbitrary

References

Angelier, J. (1979). Determination of mean principal directions of stresses for a given fault population. *Tectonophysics, 56,* T17–T26.

Angelier, J. (1989). From orientation to magnitude in paleostress determinations using fault slip data. *Journal of Structural Geology, 11*(1-2), 37–49.

Angelier, J. (1990). Inversion field data in fault tectonics to obtain the regional stress—III. A new rapid direct inversion method by analytical means. *Geophysical Journal International, 10,* 363–367.

Angelier, J., & Mechler, P. (1977). Sur une methode graphique de recherche des contraintes principales egalement utilisable en tectonique et en seismologie: la methode des diedres droits. *Bulletin de la Société géologique de France XIX, 7*(6), 1309–1318.

Burchfiel, B. C., Royden, L. H., van der Hilst, R. D., et al. (2008). A geological and geophysical context for the Wenchuan earthquake of 12 May 2008, Sichuan, People's Republic of China. *GSA Today, 18,* 4–11.

Byerlee, J. D. (1968). Brittle-ductile transition in rocks. *Journal of Geophysical Research, 73*(14), 4741–4750.

Byerlee, J. D. (1978). Friction of rocks. *Pure and Applied Geophysics*, *116*, 615–626.

Carey-Gailhardis, E., & Mercier, J. L. (1987). A numerical method for determining the state of stress using focal mechanisms of earthquake populations: Application to Tibetan teleseismic and microseismicity of Southern Peru. *Earth and Planetary Science Letters, 82,* 165–179.

Chen, Q. C., Feng, C. J., Meng, W., et al. (2012). Analysis of in situ stress measurements at the northeastern section of the Longmenshan fault zone after the 5.12 Wenchuan earthquake. *Chinese Journal of Geophysics, 55*(12), 3923–3932.

Chen, J. H., Liu, Q. Y., Li, S. C., et al. (2009). Seismotectonic study by relocation of the Wenchuan M_s 8.0 earthquake sequence. *Chinese Journal of Geophysics, 52*(2), 390–397.

Clark, M. K., & Royden, L. H. (2000). Topographic ooze: Building the eastern margin of Tibet by lower crustal flow. *Geology, 28,* 703–706.

Copley, A. (2008). Kinematics and dynamics of the southeastern margin of the Tibetan Plateau. *Geophysical Journal International, 174,* 1081–1100.

Ellsworth, W. L., & Xu, Z. H. (1980). Determination of the stress tensor from focal mechanism data. *EOS Transactions AGU, 61,* 1117.

Feng, S. Y., Zhang, P. Z., Liu, B. J., et al. (2016). Deep crustal deformation of the Longmen Shan, eastern margin of the Tibetan Plateau, from seismic reflection and finite element modeling. *Journal of Geophysical Research: Solid Earth, 121,* 767–787.

Gephart, J. W., & Forsyth, D. W. (1984). An improved method for determining the regional stress tensor using earthquake focal mechanism data: Application to the San Fernando earthquake sequence. *Journal of Geophysical Research, 89,* 9305–9320.

Gushchenko, O. I., & Kuznetsov, V. A. (1979). Determination of the orientations and the ratio of principal stresses on the basin of tectonic fault slip data. In *Stress fields in the lithosphere*, Nauka, Moscow (pp. 60–66) **(in Russian)**.

Hardebeck, J. L. (2012). Coseismic and postseismic stress rotations due to great subduction zone earthquakes. *Geophysical Research Letters, 39,* L21313.

Hardebeck, J. L., & Shearer, M. (2003). Using S/P amplitude ratios to constrain the focal mechanisms of small earthquakes. *Bulletin of the Seismological Society of America, 93*(6), 2434–2444.

Heidbach, O., Tingay, M., Barth, A., et al. (2010). Global crustal stress pattern based on the World Stress Map database release 2008. *Tectonophysics, 482,* 3–15.

Houseman, G., & England, P. (1993). Crustal thickening versus lateral expulsion in the Indian–Asian continental collision. *Journal of Geophysical Research, 98,* 12233–12249.

Kirby, E., Whipple, K., & Harkins, N. (2008). Topography reveals seismic hazard. *Nature Geoscience, 1*(8), 485–487.

Kisslinger, C. (1980). Evaluation of S to P amplitude ratios for determining focal mechanisms from regional network observations. *Bulletin of the Seismological Society of America, 70,* 999–1014.

Kisslinger, C., Bowman, J. R., & Koch, K. (1981). Procedures for computing focal mechanisms from local (SV/P) data. *Bulletin of the Seismological Society of America, 71*(6), 1719–1729.

Liang, S. H., & Li, Y. (1984). On the determining of source parameters of small earthquakes by using amplitude ratios of P and S from regional network observations. *Chinese Journal of Geophysics, 27*(3), 249–257.

Lin, J. Z., Jiang, W. Q., Li, Y. M., et al. (1991). Determination of source parameters of small earthquakes in the east part of Guangdong and South part of Fujian province. *Acta Seismologica Sinica, 13*(4), 420–429.

Liu, Q. Y., Hilst, Robert V. D., Li, Y., et al. (2014). Eastward expansion of the Tibetan Plateau by crustal flow and strain partitioning across faults. *Nature Geoscience*. https://doi.org/10.1038/ngeo2130.

Liu-Zeng, J., Zhang, Z. Q., Wen, L., et al. (2009). Co-seismic ruptures of the 12 May 2008, Ms 8.0 Wenchuan earthquake, Sichuan: East–west crustal shortening on oblique, parallel thrusts along the eastern edge of Tibet. *Earth and Planetary Science Letters, 286,* 355–370.

Michael, A. J. (1987). Use of focal mechanisms to determine stress: A control study. *Journal of Geophysical Research, 89,* 11517–11526.

Rau, R. J., Wu, F. T., & Shin, T. C. (1996). Regional network focal mechanism determination using 3D velocity model and SH/P amplitude ratio. *Bulletin of the Seismological Society of America, 86*(5), 1270–1283.

Rebetsky, Yu L, Kuchai, O. A., Sycheva, N. A., et al. (2012). Development of inversion methods on fault slip data: Stress state in orogenes of the Central Asia. *Techtonophysics, 581,* 114–131.

Rebetsky, Yu L, Polets, A Yu., & Zlobin, T. K. (2016). The state of stress in the Earth's crust along the northwestern flank of the Pacific seismic focal zone before the Tohoku earthquake of 11 March 2011. *Tectonophysics, 685,* 60–76.

Royden, L. H., Burchfiel, B. C., King, R., et al. (1997). Surface deformation and lower crustal flow in eastern Tibet. *Science, 276,* 788–790.

Royden, L. H., Burchfiel, B. C., & van der Hilst, R. D. (2008). The geological evolution of the Tibetan Plateau. *Science, 321,* 1054–1058.

Shen, Y., Forsyth, D. W., Conder, J., & Dorman, L. M. (1997). Investigation of microearthquake activity following an intraplate teleseismic swarm on the west flank of the southern East Pacific Rise. *Journal of Geophysical Research, 102*(B1), 459–475.

Snoke, J. A., Munsey, J. W., Teague, A. G., & Bollinger, G. A. (1984). A program for focal mechanism determination by combined use of polarity and SV-P amplitude ratio data. *Earthquake Notes, 55*(3), 15.

Tapponnier, P., Peltzer, G., Dain, A. Y. L., et al. (1982). Propagating extrusion tectonics in Asia: New insights from simple experiments with plasticine. *Geology, 10,* 611–616.

Tapponnier, P., Xu, Z., Roger, F., et al. (2001). Oblique stepwise rise and growth of the Tibet Plateau. *Science, 294,* 1671–1677.

von Mises, R. (1928). Mechanik der plastischen Formänderung von Kristallen. *Zeitschrift für Angewandte Mathematik und Mechanik, 8,* 161–185.

Wan, Y. G., Shen, Z. K., & Lan, C. X. (2006). Deviatoric stress level estimation according to principle axes rotation of stress field before and after large strike-slip type earthquake and stress drop. *Chinese Journal of Geophysics, 49*(3), 838–844.

Wang, F., Wang, M., Wang, Y. Z., & Shen, Z. K. (2015). Earthquake potential of the Sichuan-Yunnan region, western China. *Journal of Asian Earth Sciences, 107,* 232–243.

Xu, Z. H., Wang, S. Y., Huang, Y. R., et al. (1992). Tectonic stress field of China from a large number of small earthquakes. *Journal of Geophysical Research, 97*(B8), 11867–11877.

Xu, X., Wen, X., & Yu, G. (2009). Coseismic reverse- and oblique-slip surface faulting generated by the 2008 Mw 7.9 Wenchuan earthquake China. *Geology, 37,* 515–518.

Yang, Y. R., Johnson, K. M., & Chuang, R. Y. (2013). Inversion for absolute deviatoric crustal stress using focal mechanisms and coseismic stress changes: The 2011 M9 Tohoku-oki, Japan, earthquake. *Journal of Geophysical Research, 118,* 5516–5529.

Zhang, P. Z., Xu, X. W., Wen, X. Z., et al. (2008). Slip rates and recurrence intervals of the Longmen Shan active fault zone, and tectonic implications for the mechanism of the May 12 Wenchuan earthquake, 2008, Sichuan, China. *Chinese Journal of Geophysics, 51*(4), 1066–1073.

Zoback, M. L. (1992). First and second order patterns of stress in the lithosphere: The World Stress Map Project. *Journal of Geophysical Research: Solid Earth, 97,* 11703–11728.